Synthesis of Praseodymium-Doped TiO$_2$ Nanocatalysts by Sol-Microwave and Their Photocatalytic Activity Study

Huang Fengping,[†,*] Wang Shuai,[†] Zhang Shuang,[†] Fan Yingge,[†] Li Chunxue,[†] Wang Chuang,[‡] and Liu Chun

Xianyang Research & Design Institute of Ceramics, Xianyang 712000, P.R. China
[†]School of Chemical Engineering, Shaanxi University of Science and Technology, Xi'an 710021, P.R. China
[*]E-mail: huangfp168@163.com
[‡]Department of Highway and Bridge, Shaanxi Railway Institute, Weinan 714000, P.R. China
Received December 28, 2014, Accepted April 23, 2014

The praseodymium-doped TiO$_2$ photocatalyst samples, which could degrade methyl orange under UV irradiation, were prepared by sol-microwave method for improving the photocatalytic activity of TiO$_2$. The resulting materials were analyzed by X-ray diffraction (XRD), scanning electron microscopy (SEM), Transmission electron microscopy (TEM), X-ray photoelectron spectroscopy (XPS), Raman spectra, Fourier transform infrared spectra (FTIR) and Ultraviolet-visible diffuse reflectance spectra (UV-vis DRS). It was found Pr doping retarded the growth of crystalline size and the phase transformation from anatase to rutile, and narrowed the band gap energy. Praseodymium doping brought about remarkable improvement in the photoactivity. The optimal dopant amount of Pr was 2% by molar of cement and the calcination temperature was 500 °C for the best photocatalytic activity. The improvement of photocatalytic activity was ascribed to the occurrence of lattice distortion and the effective containment of the recombination of the electron-hole by Pr^{3+}.

Key Words : Nano-TiO$_2$, Praseodymium doped, Photocatalyst, Nanoparticle, Methyl orange

Introduction

Titanium dioxide has received a lot of attention due to its chemical stability, non-toxicity, low cost, and other advantageous properties.[1,2] It has been employed in self-cleaning, deodorant, anti-bacteria, and is expected to be applied to the pollution control to decompose toxic materials in air and waste waster. However, undoped TiO$_2$ has a band gap of 3.2 eV, which allows the oxide to absorb lights with wavelengths shorter than 385 nm. The solar light contains only a very narrow range of such high energy rays, which inhibits the utilization of solar energy in the photocatalytic process for organic treatment, and causes the invalid recombination of the photo-hole and the photo electron and low quantum efficiency.[3] In order to enhance the photocatalytic activity of TiO$_2$, it is essential for increasing the utility of TiO$_2$ by broadening the region of photo-response and inhibiting the recombination of electron-hole pairs.

Rare earth elements have separate f electron configurations and are apt to form kinds of complexes with various Lewis bases (*e.g.* acides, amines, aldehydes, alcohols, thiol, *etc.*) through interaction of these functional groups with the f-orbitals of the lanthanides. Thus, doping with lanthanide ions can provide a means to concentrate on the organic pollutant on the TiO$_2$ surface and consequently enhance the adsorption capacity.[4,5] Moreover, they can retard the transformation from anatase to rutile phase, which may be due to the stabilization of anatase phase by the surrounding rare earth ions *via* the formation of anatase-O-lanthanide bonds.[6] It is well known that anatase is beneficial to the photocatalysis. So, lanthanide ions doped TiO$_2$ has attracted researchers' great interest.[7,10] Vaclav Stengl, *et al.*[7] used the modified homogeneous hydrolysis of titania and rare earth sulphates with urea in preparation of series of photocatalysts including La^{3+}, Ce^{3+}, Ce^{4+}, Nd^{3+}, Sm^{3+}, Pr^{3+}, Eu^{3+}, Gd^{3+} and Dy^{3+} doped TiO$_2$. The doping of TiO$_2$ with rare earth ions had a considerable effect on optical properties and lead to lowers band-gap energy. The overall photocatalytic activity for Orange II dye degradation under UV or visible-light irradiation was significantly enhanced by doping with the rare earth ions, which was caused by higher adsorption, and the 4f electron transition of rare earth ions. Jing *et al.*[8] researched La-doped TiO$_2$ nanoparticles and investigated their photocatalytic activity for degrading phenol. The results showed that La^{3+} did not enter into the crystal lattices of TiO$_2$ and was uniformly dispersed in TiO$_2$ as the form of La$_2$O$_3$ particles with small size, which possibly made La dopant have a great inhibition on TiO$_2$ phase transformation. Ji *et al.*[9] prepared rare earth (Er^{3+} or Yb^{3+}/Er^{3+})-doped TiO$_2$ nanobelts under hydrothermal process. The results demonstrated that the rare earth ions have doped into the lattice of TiO$_2$, and the Er^{3+} or Yb^{3+}/Er^{3+}-doped nanobelts showed strong visible up-conversion (UC) fluorescence under 980 nm excitation.

In the present work, Pr-doped TiO$_2$ nanocrystals were successfully synthesized by the sol-microwave method. The characterization of the prepared samples were analyzed by XRD, SEM, TEM, XPS, Raman spectra, FTIR and UV-vis DRS. The photocatalytic properties were evaluated by the degradation of methyl orange in TiO$_2$ aqueous solution under UV irradiation. The excellent photocatalytic activity of Pr-doped TiO$_2$ was compared to pure TiO$_2$. The influence

of praseodymium ion dosage and calcinations temperature on the photoactivity was investigated.

Experimental

Materials. Tetra-*n*-butyl titanate and $Pr(NO_3)_3 \cdot 6H_2O$ with analytical grade were obtained from Kermel Chemical Co. The chemically pure methyl orange was purchased from Damao Chemicals Co. Anhydrous ethanol and diethanol amine and all other chemicals were of analytical reagent grade, and used without further purification. De-ionized water was used throughout this study.

Preparation of Samples. First, the sample was prepared *via* a sol-microwave route as follows. In this method, Tetra-*n*-butyl titanate was mixed with anhydrous ethanol. Appropriate amount of diethanol amine was added to this mixture under constant stirring. The molar ratio of tetra-*n*-butyl titanate: anhydrous ethanol: diethanol amine was 4:15:1. Next, in this solution, a mixture of de-ionized water and anhydrous ethanol was added by drop using a burette. The solution was stirred for 30 mins to get a yellow transparent sol. Then the sol was under microwave (Galanz, 2.45 Hz, 800W) irradiation (40% power) for 4 min. The white gel product was filtered, washed with distilled water and dried in oven for several hours. Finally, it was calcined at various temperatures from 400 to 600 $^{\circ}$C in air for 6 h. To prepare Pr-doped TiO₂, the above procedure was repeated, including praseodymium nitrate to the drop-wise addition of water-anhydrous ethanol solution.

Characterization Methods. The crystalline phase of the samples was analyzed by XRD (Shimadzu D/max-2200/PC) with a Cu Kα radiation ($\lambda = 0.15406$ nm) with $2\theta = 10^{\circ}$ …70°, the graphite monochromator and scans at 8 ($^{\circ}$)/min. Scanning electron microscopy (SEM) of the as-formed surface and thermally etched cross-sections was performed using a Hitachi S4800. The particulate morphology of the samples was observed on TEM (Hitachi-H7650) at 190 kV. To investigate their chemical states, X-ray photoelectron spectroscopy (XPS) was performed with PerkinElmer PHI-5400 System with Al (Kα) source (hν = 1486.6 eV). A flood gun was used to neutralize the sample surface, while the C (1s) line was used for a final energy scale calibration. To investigate the changes in the local structure of the TiO₂ photocatalysts, FT-IR spectra were monitored by spectrum 100, Perkin Elmer (USA). The ultraviolet-visible diffuse reflectance spectra (UV-vis DRS) of the samples in the wavelength range 250-750 nm were recorded using a spectrophotometer(Shimadzu UV-2450), with BaSO₄ as a reference. Raman measurements were performed at room temperature using a Via+ Reflex Raman spectrometer with the excitation light of 514 nm.

Photocatalytic Activity. The photocatalytic activity of each simple was evaluated by the degradation of methyl orange in TiO₂ aqueous solution under UV irradiation. A 300 W high pressure Hg lamp for which the predominated irradiation wavelength was 365 nm was used as a UV light source. The photocatalyst (0.10 g) was added into a 100 mL

quartz photoreactor containing 80 mL of a 1.0×10^{-4} gL^{-1} methyl orange solution. The photoreactor was cooled with flowing water in a quartz cylindrical jacket around the reactor, and ambient temperature was maintained at 10 $^{\circ}$C during the photocatalytic reaction. The suspension was stirred in dark for 30 min to reach the adsorption-desorption equilibrium. Then it was irradiated under UV. The samples were withdrawn periodically from the reactor, centrifuged and analyzed by recording variations in the absorption in the UV-vis spectra of methyl orange using a Cary 500 UV-vis spectrophotometer at its characteristic wavelength ($\lambda = 465$ nm).

Results and Discussion

XRD Analysis. XRD is usually used for identification of the crystal phase and the estimation of the ratio of the anatase to rutile as well as the crystallite size of each phase present. The X-ray diffraction patterns as seen in Figure 1 were provided to find out the optimum condition of the Pr-doped TiO₂ for different Pr contents of 0.5, 1.0, 2.0, 3.0, and 4.0% by molar of cement. The sharpest diffraction peaks marked in "A" in Figure 1 are the remarks of anatase and the peaks symbolized in "R" stand for the rutile, which showed that all catalysts were dominated by anatase TiO₂. With respect to Pr-doped TiO₂ samples, the peak of rutile was disappeared with the increasing praseodymium ion dosage. This indicated that praseodymium ion doping inhibited the
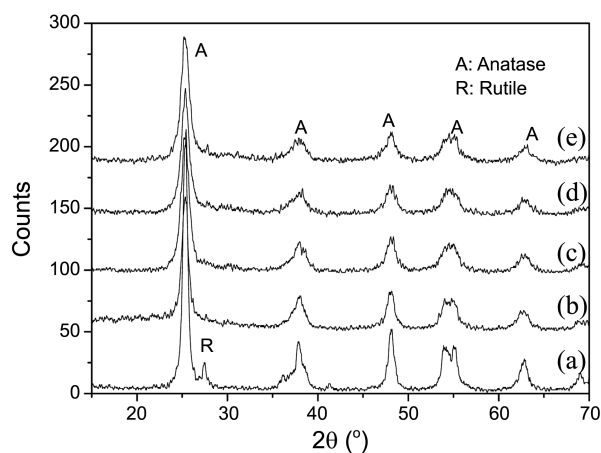

Figure 1. XRD patterns of different samples calcined at 500 $^{\circ}$C: (a) 0.5% Pr-doped TiO₂, (b) 1.0% Pr-doped TiO₂, (c) 2.0% Pr-doped TiO₂, (d) 3.0% Pr-doped TiO₂, (e) 4.0% Pr-doped TiO₂.

Table 1. Crystallite size of Pr-doped TiO₂ containing different praseodymium content calcined at 500 $^{\circ}$C

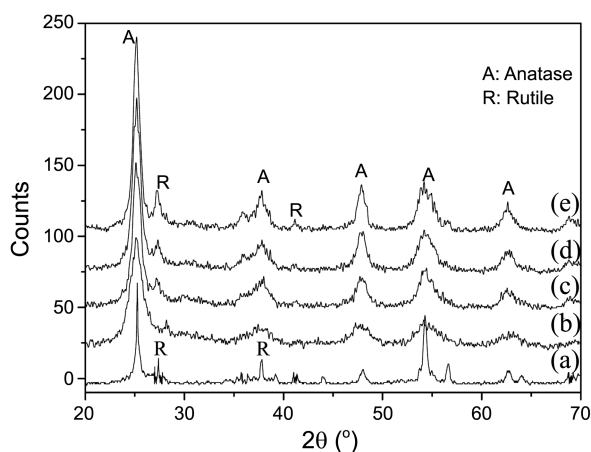| Sample	Crystallite size D/(nm)
(0.5%)Pr-doped TiO₂	14.4
(1.0%)Pr-doped TiO₂	11.6
(2.0%)Pr-doped TiO₂	10.0
(3.0%)Pr-doped TiO₂	9.4
(4.0%)Pr-doped TiO₂	8.9

Figure 2. XRD patterns of different samples calcined at different temperatures: (a) pure TiO_2-400 °C, (b) Pr-doped TiO_2-400 °C, (c) Pr-doped TiO_2-500 °C, (d) Pr-doped TiO_2-550 °C, (e) Pr-doped TiO_2-600 °C.

Table 2. Crystallite size of pure TiO_2 and 2% Pr-doped TiO_2 calcined at different temperature

Sample	Crystallite size D/(nm)
pure TiO_2-400 °C	21
Pr-TiO_2-400 °C	9.2
Pr-TiO_2-500 °C	10.0
Pr-TiO_2-550 °C	11.4
Pr-TiO_2-600 °C	12.9

phase transformation from anatase to rutile phase in the solid. The average size of crystallite was calculated from the (101) peak of anatase TiO_2 in accordance with the Scherrer equation:[11]

$$D = K/\cos\theta \qquad (1)$$

where D is the crystallite size, refers to the full width half maximum (FWHM) of the 2θ peak, K signifies the shape factor of the particles (it equals to 0.89), θ and λ stand for the incident of angle and the wavelength of the X-rays, respectively. As shown in Table 1, the crystallite size significantly decreased with increasing the dosage of praseodymium. The 4.0% Pr-doped TiO_2 sample only had a crystallite of 9.4 nm. This reduction in crystallite size was proposed to be due to segregation of the praseodymium cations at the grain boundary, which restrained the grain growth by restricting direct contact of grains.[12] Besides, the dosage of praseodymium ion, the annealing temperature also exerted an effect on the crystallinity of the as-prepared photocatalysts. Figure 2 showed the XRD patterns of pure TiO_2 and Pr-doped TiO_2 calcined at different temperatures when the samples were doped with 2.0% praseodymium. It can be seen that the rutile phase appeared for pour TiO_2 at 400 °C, whereas a little rutile phase appeared for Pr-doped TiO_2 at the calcining temperature of 600 °C. The result showed that the Pr-doped not only greatly retarded the phase transformation from anatase to rutile, but enhanced the initial temperature of

phase transformation obviously and improved the high-temperature anatase phase stability of TiO_2 by the surrounding praseodymium ions through the formation of Ti-O-Pr bonds.[13] The crystallite size of Pr-doped TiO_2 became smaller than that of pure TiO_2 as shown in Table 2, which was caused by segregation of the Pr^{3+} at the grain boundary. With increasing calcination temperature, the crystallite size of Pr-doped TiO_2 significantly became larger, demonstrating that the calcining temperature had a great impact on the properties of Pr-doped TiO_2 samples during the preparation process.

SEM and TEM Analysis. The morphological characterization of pure TiO_2 and Pr^{3+} doped TiO_2 nanoparticles were carried out by SEM and TEM as shown in Figure 3(a) and 3(c) were the SEM and TEM photographs of pure TiO_2 calcined at 400 °C. The pure TiO_2 nanoparticles exhibited irregular morphology and the diameter was more than 20 nm. However, Pr-doped TiO_2 had uniform spherical shape and size with an average diameter of 10.0 nm or so (Figure 3(b), Figure 3(d)), which was in good agreement with the XRD evaluation (Table 1). The reunion phenomenon of Pr-doped TiO_2 particle was more serious because of small particle size. The results implied that Pr dopant could inhibit the increase of TiO_2 particle size. The energy dispersive X-ray (EDX) spectrum was further used to analyze the composites of the as-obtained Pr-doped TiO_2 nanoparticles, and the result was shown in Figure 4 Ti, O and Pr peaks were observed in these spectra together with weak C peak (the peak of C came from residual organic matter after calcinations). The contents of O, Ti and Pr elements were 43.24 at%, 35.63 at% and 1.5 at%, respectively.

XPS Analysis. Pr-doped TiO_2 was further analyzed by XPS as shown in Figure 5 to determine the main elements and chemicals state on the TiO_2 surface. In Figure 5(a), XPS peaks showed four elements, namely, Ti, O, Pr and C, were present together on the TiO_2 surface. Pr came from the doping solution, and C probably originated from the calcinations
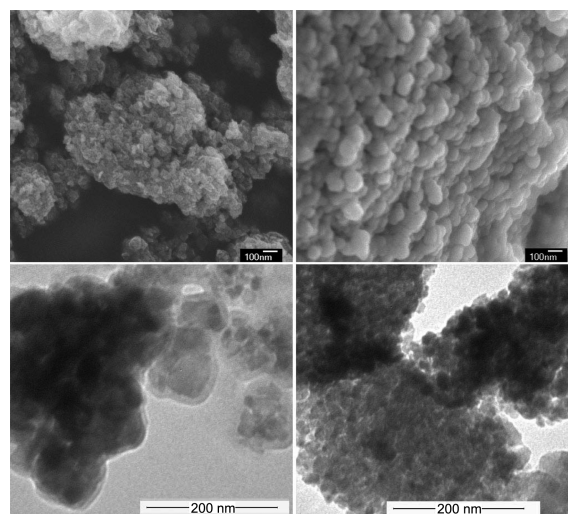

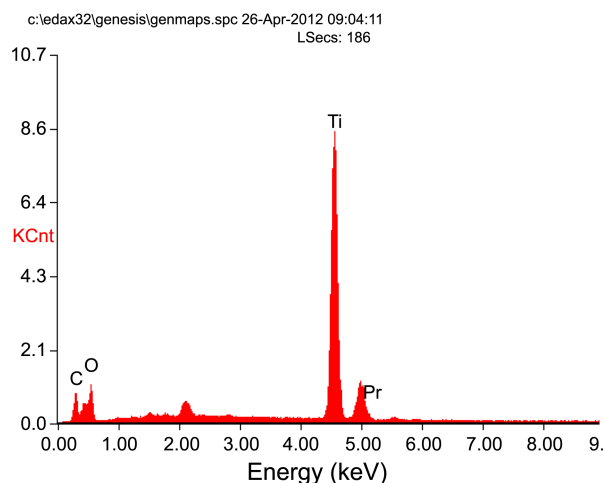**Figure 3.** SEM images of (a) pure TiO_2 (b) Pr-doped TiO_2 and TEM images of (c) pure TiO_2 (d) Pr-doped TiO_2.

Study of Praseodymium Doped on the Nanosized TiO$_2$ Catalyst

Bull. Korean Chem. Soc. **2014**, Vol. 35, No. 8   2515

Figure 4. EDS spectrum of TiO$_2$ nanoparticles doped with Pr^{3+}.

Table 3. Molar ratio of Pr/Ti from XPS in Pr-TiO$_2$ calcined at 500 °C

sample	Pr/Ti theoretically (at%)	Pr/Ti analyzed by XPS (at%)
Pr-TiO$_2$-500	2%	4.9%

could be fitted into two peaks. The peak at 934.67 eV (Pr3d$_{5/2}$) was corresponding to the bond of Pr-O, and was assigned to the Pr atoms from Pr$_2$O$_3$. That at 953.2 eV was corresponding to the bond of Pr-O-Ti. The atomic contents of praseodymium in samples calcined at 500 °C were calculated from XPS peak areas and were given in Table 3. It was found to be 4.9 at% of praseodymium for 2% Pr -TiO$_2$. As seen in Table 3, it is clearly seen that the atomic ratio of Pr/Ti clearly increase. The result shows that the content of the doped Pr through surface concentration. Because the ionic radius of Pr^{3+} (0.1013 nm) was bigger than the ionic radius of Ti^{4+} (0.068 nm) and the Pr^{3+} ions couldn't enter into the lattice of TiO$_2$, Ti^{4+} ion might enter into the lattice of the Pr$_2$O$_3$ which could cause the change of electron field of Pr^{3+} and increase the electron density, and hence decrease the binding energy of Pr^{3+}.

Raman Analysis. The Raman spectra of samples were shown in Figure 6. Anatase TiO$_2$ was D$^{19}_{4h}$ (*I4$_1$/amd*) space groups, containing two TiO$_2$ molecules in each unit cell, and raman vibrational mode was A$_{1g}$+2B$_{1g}$+3E$_g$, while rutile TiO$_2$ was D$^{14}_{4h}$ (*P4$_2$/mnm*) space groups, and raman vibrational mode was A$_{1g}$+B$_{1g}$+B$_{2g}$+E$_g$. The Raman spectrum for anatase TiO$_2$ was identified at 144 cm^{-1}(B$_{1g}$), 196 cm^{-1}(B$_{1g}$), 325 cm^{-1}(E$_g$), 398 cm^{-1}(E$_g$), 516 cm^{-1}(E$_g$), 638 cm^{-1}(A$_{1g}$) and rutile TiO$_2$ was 144 cm^{-1}(B$_{1g}$), 236 cm^{-1}(E$_g$), 446 cm^{-1} (E$_g$), 610 cm^{-1}(A$_{1g}$) by the standard pattern.[19] The Raman spectrum of the pure TiO$_2$ crystal showed peaks at 140.703 cm^{-1}(B$_{1g}$), 394.132 cm^{-1}(E$_g$), 514.323 cm^{-1}(E$_g$) and 635.017 cm^{-1} (A$_{1g}$) (Figure 6(a)), indicating that anatase nanoparticles are the predominant species. The additional peak at 444.336 cm^{-1}(E$_g$) was observed in the spectra of pure TiO$_2$ indicating that there is still rutile phase in the sample. The results were consistent with the XRD measurements. The 140.703 cm^{-1} peak was E$_g$ symmetric type of O-Ti-O variable angle vibration peak and had a maximum strength. The spectra of praseodymium iron doped TiO$_2$ nanocrystals were
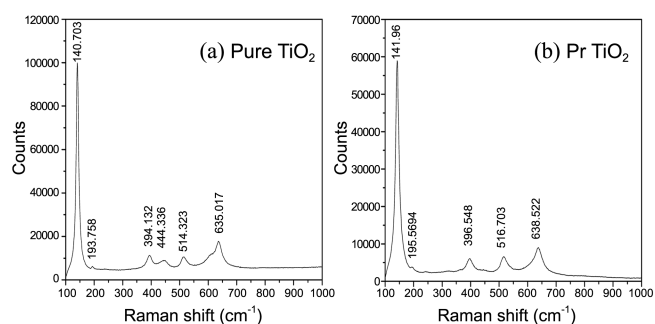

Figure 5. (a) XPS survey spectrum of Pr-doped TiO$_2$ calcined at 500 °C; (b)-(d) high-resolution XPS spectra of O1s, Ti2p and Pr3d for Pr-doped TiO$_2$ sample.

residue of organic precursor. Figure 5(b) showed the Ti2p XPS spectra of Pr-doped TiO$_2$ sample. The binding energies of peaks of Ti2p$_{1/2}$ and Ti2p$_{3/2}$ were 464.58 eV and 458.78 eV, respectively. The distance of peaks between Ti2p$_{1/2}$ and Ti2p$_{3/2}$ was 5.8 eV, which indicated the titanium mainly existed as Ti^{4+}.[14] According to other literature and XPS handbook,[15,16] the Ti2p$_{3/2}$ core levels of pure TiO$_2$ appeared at 459.05 eV. Similar shift was previously attributed to the change of the local chemical environment of Ti ions influenced by praseodymium incorporation and to the formation of Pr-O-Ti bonds on the TiO$_2$ surface.[17,18]

The O1s XPS spectra were broad and asymmetric (Figure 5(c)), indicating the existence of more than one chemical state convoluted in these spectra. There were three O1s peak components. The O1s peak at 529.98 eV was the characteristic peak of lattice oxygen (Ti-O bond), at 532.28 eV was the chemisorbed surface hydroxyl oxygen (O-H bond), and at 530.07 eV represented the Pr-O bond in Pr$_2$O$_3$ form.

Figure 5(d) showed the XPS spectrum of Pr3d. The curve

Figure 6. Raman spectra of (a) pure TiO$_2$ calcined at 400 °C and (b) Pr-doped TiO$_2$ calcined at 500 °C.
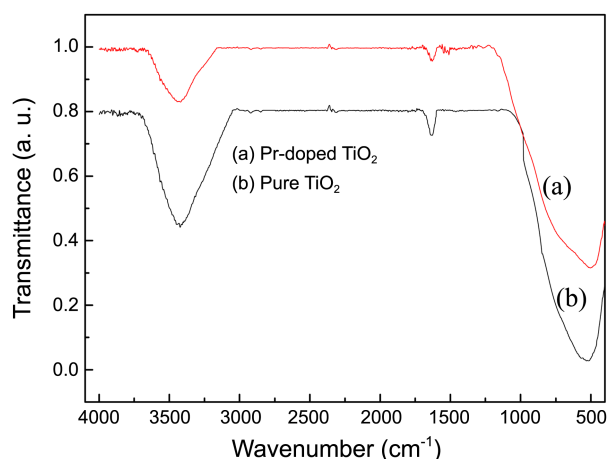
Figure 7. FT-IR spectra of (a) Pr-doped TiO₂ and (b) pure TiO₂.

similar to those of anatase but being slightly red shifted which was attributed to reduction in TiO₂ particle size, phonon confinement, oxygen deficiency, and pressure effects.[20] Moreover, no Raman lines corresponding to rutile TiO₂ were observed in the Pr-doped TiO₂ calcined at 500 °C. The results were in agreement with the XRD measurements.

FTIR Analysis. Figure 7 showed the FT-IR spectra of the prepared pure TiO₂ and Pr-doped TiO₂ in the region between 400 and 4000 cm⁻¹. There were mainly three absorption bands in the region of 500-550 cm⁻¹, 1620-1630 cm⁻¹, 3400-3420 cm⁻¹ for the two samples. In the low energy region, both the FT-IR spectra of pure TiO₂ and Pr-doped TiO₂ showed a characteristic peak of titania at about 520 cm⁻¹, which was assigned to the stretching vibration of Ti-O,[21] corresponding to the presence of TiO₆ group. For Pr-doped TiO₂, a broad peak at about 3400 cm⁻¹ occurred, assigned to the stretching vibration mode of the O-H groups of physical absorbed molecular water, and a corresponding weak bending vibration band at near 1620 cm⁻¹ was also observed.[22] These peaks of Pr-doped TiO₂ became much stronger than those of pure TiO₂, implying that the surface of the doped samples might attract more hydroxyl and have strong adsorption. A large number of hydroxyl was conducive to the process of photo-catalytic reaction. The hydroxyl could capture the photo-generated holes (h⁺) to generate hydroxyl radicals (·OH) after light irradiation, while hydroxyl radicals had high oxidative capacity.

UV-vis DRS Analysis. To study the optical absorption properties of catalysts, diffuse reflectance absorption spectra (DRS) in the range of 220-800 nm were investigated and the results were shown in Figure 8, from which it can be seen that pure TiO₂ had no absorption in the visible light region (> 400 nm), while Pr-doped TiO₂ catalyst displayed a weak absorption band in the range of 400-600 nm. The broad bands at 400-500 nm can be ascribed to f→f transition while the weak absorption at around 600 nm was ascribed to the characteristic transition of Pr^{3+} $D_2 \rightarrow ^3H_4$.[23] Pr-doped enhanced the visible light utilization efficiency and triggered about 50 nm red shift of absorption spectra compared to pure TiO₂. Kubelka-Munk function was used to estimate the band gap
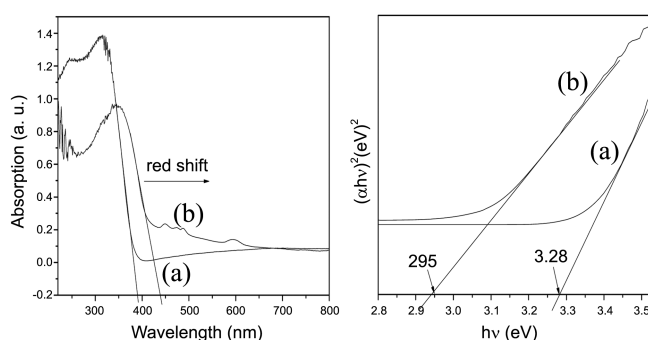

Figure 8. DRS spectra of (a) pure TiO₂ and (b) Pr-doped TiO₂ nanoparticles.

energy of the prepared samples by plotting $(\alpha h\nu)^{1/2}$ versus energy of light (saw Figure 8(b)). Results indicated that the band gap energy of pure TiO₂ was 3.28 eV, and with the doping of praseodymium, the red shift was observed in the Pr-doped TiO₂ and the band gap energy of Pr-doped TiO₂ was 2.95 eV, showing that the band gap of TiO₂ could reduce. This might be caused by the following reasons: (a) Pr intervention changed the original ligand field of TiO₂, and further enhanced the Stark effect, which made the TiO₂ band gap narrow and caused red shift in the absorption of ultraviolet light; and (b) as soon as Pr-doped TiO₂ absorbed ultraviolet light, the energy could be transferred to the titanium dioxide by electron transfer, leading to its red shift in the absorption of ultraviolet light.[24]

Photocatalytic Activity.

Effect of Annealing Temperature: The photocatalytic activities of 2% Pr-doped TiO₂ calcined at different temperature from 400 °C to 600 °C were shown in Figure 9. It can be found that the sample calcined at 500 °C exhibited the highest photocatalytic activity which could nearly reach 73.10% in an hour, indicating that 500 °C was the most appropriate calcination temperature. At lower annealing temperature, Pr-doped TiO₂ had a mass of surface hydroxyl, which made the recombination probability of electron-hole
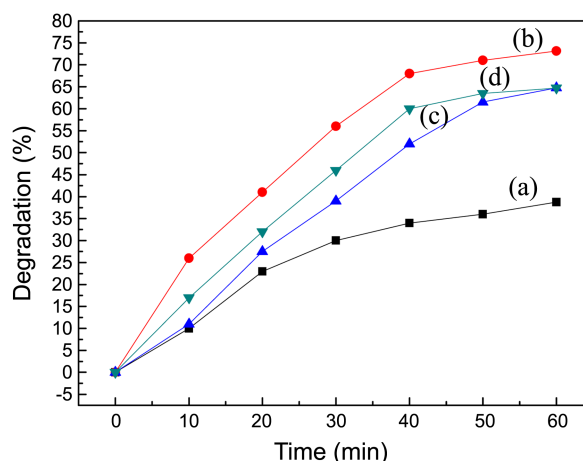

Figure 9. Photocatalytic degradation of methyl orange using 2.0% Pr-doped TiO₂ calcined at different temperatures: (a) 400 °C, (b) 500 °C, (c) 550 °C, (d) 600 °C
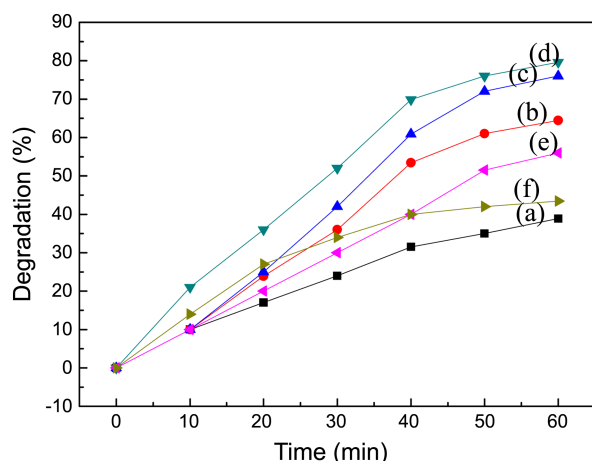
Figure 10. Photocatalytic degradation of methyl orange using different samples calcined at 500 °C: (a) pure TiO₂, (b) 0.5% Pr-doped TiO₂, (c) 1.0% Pr-doped TiO₂, (d) 2.0% Pr-doped TiO₂, (e) 3.0% Pr-doped TiO₂, (f) 4.0% Pr-doped TiO₂.

increase. At the same time, when the temperature was too low, the catalyst reduced its catalytic ability due to large particle size and small specific surface.[25] And with the increase of calcination temperature, the crystallinity of photocatalysts became better and better and the crystal form of TiO₂ transformed from amorphous to anatase, so the photocatalytic activity increased. As the calcination temperature continued to rise, the particle size increased, and the lattice distortion reduced and weakened the adsorption capacity of oxygen. The adsorbed oxygen could capture optical-electronic in a photocatalytic process and inhibit the recombination of electron-hole, which increased its photocatalytic activity. Therefore, it was easy to understand that the sample 2% Pr-doped TiO₂ calcinated at 500 °C exhibited the highest photocatalytic performance for methyl orange decomposition under ultraviolet light illumination.

Effect of Praseodymium: The photocatalytic degradation of methyl orange under ultraviolet light irradiation over different samples was evaluated and the results were shown in Figure 10. Obviously, the photocatalytic efficiency of the samples was strongly dependent on the dopant amount of praseodymium. The photocatalytic activity of Pr-doped TiO₂ was apparently higher than that of pure TiO₂ and the 2% Pr-doped TiO₂ exhibited the highest photocatalytic activity which could nearly reach 79.62% in an hour. This was because praseodymium ions radius (0.1013 nm) was greater than that of Ti^{4+} (0.068 nm). So, it was difficult for Pr^{3+} to enter the TiO₂ lattice to form solid solution. However, Ti^{4+} was an alternative to replace Pr^{3+}, caused by electric charge imbalance. In order to compensate for this imbalance, more hydroxide ions adsorbed on the TiO₂ surface to enhance photocatalytic activity. According to the band theory of solid state physics, the lattice distortion can produce the lattice strain. In order to compensate for this lattice stress, the oxygen atoms of TiO₂ lattice surface easily fled lattice to capture the holes. Lattice distortion could reduce the recombination probability of electron-hole and thus improve

the photocatalysis. When the dopant concentration was more than 2%, the photocatalytic activity decreased, which implied that the lower doping amount led to the insufficient number of shallow potential wells used to capture electrons or holes. So, the photogenerated electron-hole pairs could not effectively separate. But the doping level was too high; the metal ions might become electron-hole recombination centers, thereby increasing the composite probability of electrons and holes, the photocatalytic degradation efficiency decreased. After Pr doping, TiO₂ particle became smaller, the specific surface was increased, and the quantum chemical effects became more apparent. These factors were beneficial to improve the photocatalytic activity of TiO₂ particles.

Conclusion

(1) Photocatalyst of Pr-doped TiO₂ was successfully prepared by sol-microwave method. With respect to Pr-doped TiO₂ samples, the characteristic peak of crystal plane (101) of anatase became broader and the relative intensity decreased with increasing praseodymium ion dosage. The 4.0% Pr-doped TiO₂ sample only had a crystallite of 9.4 nm. The praseodymium doping inhibited the anatase-to-rutile phase transformation, and the rutile phase appeared for Pr-doped TiO₂ at the calcining temperature of 600 °C. Whereas, for the pour TiO₂, the rutile phase appeared at 400 °C. The catalyst of Pr-doped TiO₂ calcined at 500 °C was dominated by anatase TiO₂.

(2) Pr-doped enhanced the visible light utilization efficiency and triggered about 50 nm red shift of absorption spectra compared to pure TiO₂. The band gap energy of pure TiO₂ was 3.28 eV, and with the doping of praseodymium, the red shift was observed in the Pr-doped TiO₂ and the band gap energy of Pr-doped TiO₂ was 2.95 eV, showing that the band gap of TiO₂ could reduce.

(3) The highest enhancement in photocatalytic activity was obtained with 2% praseodymium doping and calcined at 500 °C. The photocatalytic activity of Pr-doped TiO₂ was highly improved compared to pure TiO₂ for methyl orange degradation under UV irradiation. This high activity was attributed to produce the lattice distortion and inhibit efficiently of the recombination of the electron-hole by Pr^{3+}.

References

1. Rajesh, J. T.; Ramchandra, G. K. *Ind. Eng. Chem. Res.* **2006**, *45*, 922.
2. Reijnders, L. *J. Hazard. Mater.* **2008**, *152*, 440.
3. Anil, K.; Arvind, K. J. *J. Photochem. Photobiol. A* **2003**, *156*, 207.
4. Xiao, Q.; Zhang, J.; Xiao, C.; Si, Z. C.; Tan, X. K. *J. Hazard. Mater.* **2008**, *150*, 62.
5. Parida, K. M.; Nruparaj, S. *J. Mol. Catal. A: Chem.* **2008**, *287*,

151.

6. Li, J. H.; Yang, X.; Yu, X. D.; Xu, L. L. *Appl. Surf. Sci.* **2009**, *255*, 3731.

7. Vaclav, S.; Snejana, B.; Nataliya, M. *Mater. Chem. Phys.* **2009**, *114*, 217.

8. Jing, L. Q.; Sun, X. J.; Xin, B. F. *J. Solid State Chem.* **2004**, *177*, 3375.

9. Ji, T. H.; Liu, Y.; Zhao, H. *J. Solid State Chem.* **2010**, *183*, 584.

10. Li, H. B.; Sheng, Y.; Zhang, H. G. *Powder Technol.* **2011**, *212*, 372.

11. Zhang, Q. H.; Gao, L.; Guo, J. K. *Appl. Catal. B: Environ.* **2000**, *26*, 207.

12. Ding, X. Z.; Liu, X. H. *J. Mater. Res.* **1998**, *13*, 2556.

13. Arbiol, J.; Cerda, J.; Dezanneau, G. *J. Appl. Phys.* **2002**, *92*, 853.

14. Yang, J.; Dai, J.; Li, J. T. *Appl. Surf. Sci.* **2011**, *257*, 8965.

15. Huang, D. G.; Liao, S. J.; Zhou, W. B. *J. Phys. Chem. Solids* **2009**, *70*, 853.

16. Ma, Y. F.; Zhang, J. L.; Tian, B. Z. *J. Hazard. Mater.* **2010**, *82*, 386.

17. Crepaldi, E. L.; Soler-Illia, G. J. D. A. A.; Grosso, D. *J. Am. Chem. Soc.* **2003**, *125*, 9770.

18. Sunil, D. S.; Saini, K. K.; Chander, K. *Appl. C. B: Environ.* **2008**, *84*, 233.

19. Wang, J. Q.; Xin, B. F.; Yu, H. T. *Chem. J. Chinese Universities* **2003**, *24*, 1237.

20. Porkodi, K.; Arokiamary, S. D. *Mater. Charact.* **2007**, *58*, 495.

21. Liu, S.; Chen, X.; Chen, X. *Chin. J. Catal.* **2006**, *27*, 697.

22. Camilo, A. C.; Aristobulo, C.; Sonia, A. *Giraldo. Mater. Chem. Phys.* **2011**, *129*, 1176.

23. Liang, C. H.; Li, F. B.; Liu, C. S. *Dyes Pigments* **2008**, *76*, 477.

24. Wang, Q. Q.; Xu, S. H.; Shen, F. L. *Appl. Surf. Sci.* **2011**, *257*, 7671.

25. Yang, W.; Hao, G.; Zhang, W. H. *Spectrosc. Speci. Anal.* **2008**, *4*, 922.